JOURNAL OF PROPULSION AND POWER
Vol. 27, No. 1, January–February 2011

Thrust Nozzle Design Study for a Quasi-Axisymmetric Scramjet-Powered Vehicle

Katsuyoshi Tanimizu,* David J. Mee,† Raymond J. Stalker,‡ and Peter A. Jacobs§
University of Queensland, Brisbane, Queensland 4072, Australia

DOI: 10.2514/1.48586

The design of a nozzle of an unfueled quasi-axisymmetric scramjet model is optimized for minimum drag for a Mach 8 flight condition. The approach to the nozzle design is to develop a simple force-prediction methodology in an optimization study. The study is completed for an unfueled configuration, but the approach could be used for fueled configuration by including appropriate combustion modeling. The effects of the nozzle design on the overall vehicle performance are included. The overall drag of the baseline model for the optimization study was measured in the T4 shock tunnel for Mach numbers ranging from 5.7 to 10.3, confirming the suitability of the force-prediction methodology. The results of the nozzle-optimization study show that performance is limited by the nozzle area ratio that can be incorporated into the vehicle without leading to too large of a base diameter of the vehicle and increasing the external drag of the vehicle. The drag of vehicle designs at different flight Mach numbers is investigated in a parametric study for Mach numbers from 6 to 10. The results confirm that longer nozzles are better at higher Mach numbers.

Nomenclature

A	=	area, m^2
C_D	=	drag coefficient
C_{TN}	=	thrust coefficient
D	=	measured axial force, N
F_p	=	pressure force, N
F_v	=	viscous force, N
L	=	length, m
M	=	freestream Mach number
p	=	pressure, kPa
Q	=	heat released by the fuel
R	=	specific gas constant, $J/(kg \cdot K)$
Re	=	Reynolds number
T	=	temperature, K
U	=	freestream velocity, m/s
γ	=	ratio of specific heats
ρ	=	freestream density, kg/m^3

Subscripts

a	=	ambient
c	=	combustion chamber
exit	=	exit
i	=	intake
s	=	separation
∞	=	freestream

Received 21 December 2009; revision received 21 August 2010; accepted for publication 21 August 2010.

*Research Fellow, School of Mechanical and Mining Engineering, Centre for Hypersonics, School of Mechanical and Mining Engineering.

†Professor, School of Mechanical and Mining Engineering, Centre for Hypersonics, School of Mechanical and Mining Engineering. Associate Fellow AIAA.

‡Emeritus Professor, School of Mechanical and Mining Engineering, Centre for Hypersonics, School of Mechanical and Mining Engineering. Fellow AIAA.

§Senior Lecturer, School of Mechanical and Mining Engineering, Centre for Hypersonics, School of Mechanical and Mining Engineering.

I. Introduction

SCRAMJET-POWERED vehicles, with an axisymmetric centerbody and either an annular combustor or several combustion chambers arranged around the centerbody, have been investigated by several researchers (e.g., [1–3]). This type of configuration is attractive for a scramjet-powered vehicle, because it includes an internal volume for a payload and has the combustion chambers arranged externally around the vehicle centerbody so that it can effectively radiate heat away. Such a vehicle could form a stage of a launch vehicle. Paull et al. [3] demonstrated that such a quasi-axisymmetric scramjet vehicle could produce enough thrust to overcome drag, over a limited range of conditions, in tests in the T4 Stalker tube [4] at the University of Queensland. They analyzed the performance of the vehicle by comparing the measurements with results from simple hypersonic theory with appropriate modeling assumptions. They suggest that the overall performance of this type of vehicle could be improved by incorporating a more effective nozzle. To test this hypothesis, a nozzle-optimization study is reported here.

The difference between the thrust and the drag of a scramjet-powered vehicle can be a small amount relative to the total drag so that relatively small changes in either can lead to large differences in the performance of the vehicle. It is, therefore, important to be able to predict accurately the performance of components of scramjet-powered vehicles and to account for the interactions between components. The flow through the engines and around the vehicles can be complex and three-dimensional (3-D) viscous computational fluid dynamics (CFD) is often used to evaluate the performance of a vehicle design [5]. Optimization over a range of conditions can be used to design high-performance vehicles, but is restricted by the large computation times when optimization includes full CFD simulations. Therefore, simpler and more computationally efficient prediction methodologies are attractive for design optimization studies.

To develop a simple but adequately accurate force predicting methodology, a quasi-axisymmetric scramjet model designed for Mach 6 flight conditions was tested in the T4 shock tunnel over a range of test conditions. The results from the force-prediction methodology developed were compared with the experimental results of Paull et al. [3]; this is reported elsewhere [6]. The force-prediction methodology, that incorporates some inviscid CFD modeling of the nozzle flow, was able to predict the performance of two, similar quasi-axisymmetric scramjets for Mach numbers ranging from 5.8 to 10 and varying Reynolds number.

The purpose of this paper is to investigate the possibility of the improvement of this type of vehicle design via a nozzle shape

optimization for a Mach 8 design condition. There have been a number of axisymmetric scramjet-powered vehicle design studies that have concentrated on optimization of the engine inlets (e.g., [7–9]), but fewer have concentrated on optimization of thrust nozzles (e.g., [1,10]). Therefore, the present study was directed at investigating thrust nozzle design. This involved investigating the effects of varying the length of the nozzle and the amount of external deflection of the cowl and the shape of the splitters and centerbody.

The goal is to minimize the drag of the vehicle for fuel-off conditions. The axial thrust of a nonlifting scramjet vehicle can be written as (Stalker et al. [11])

$$C_{TN} = \frac{2\Delta Q}{U^2}\left(1 - \frac{0.5\Delta Q}{U^2}\right) - C_D \tag{1}$$

where C_{TN}, ΔQ, U, and C_D are the thrust coefficient, heat released by the fuel, the flight speed and the vehicle's drag coefficient, respectively. This shows explicitly how the thrust coefficient depends on the drag coefficient. Thus, the design study for an unfueled version of the vehicle is a useful step in the overall design process. The effect of combustion can be regarded as an increase in temperature as the flow passes through the combustion chamber with an increase in pressure and a possible variation in the specific heats. Thus, one of the major effects of combustion is a change in the Mach number of the flow passing into the thrust nozzle implying that the nozzle-optimization procedures presented here may also be applied to situations involving combustion, but with a nozzle entry Mach number that is different from that appropriate to the no-combustion cases presented here. Note also that there are other effects of combustion, such as changes in viscous drag, that may also occur. To complete the optimization process for the combustion case requires that an optimum choice be made between the nozzles suitable for the nozzle entry Mach number with combustion and without combustion, but this is not considered here. Therefore, in this study, the analysis and experiments are done with unfueled scramjet models in order to demonstrate the optimization of the vehicles while avoiding the complexities introduced by combustion mechanisms. In addition, the experimental test models used in this study are not large enough for combustion because of relatively short combustors. Therefore, a minimum net drag, instead of a maximum net thrust, is the objective function for the optimization study. The overall performance with combustion can be estimated by combining results from this study with results from a combustion analysis. This approach has been demonstrated to be suitable in Paull et al. [3].

There are also a number of other issues that can arise when modeling combustion. For example, Stalker et al. [12] investigated the effects of nonequilibrium chemistry freezing, which occurs when a chemically reacting gas undergoing a rapid expansion in a nozzle from an equilibrium state, is unable to adjust its composition rapidly enough to maintain equilibrium. The composition of the gas freezes at some point in the nozzle expansion process. Another possibility is kinetic afterburning, which takes place when the combustion reactions are unable to approach chemical equilibrium in the combustion chamber before they encounter the falling pressure and temperature in the nozzle and combustion continues in the lower temperature expanded flow in the nozzle. In the case of nozzle freezing, Stalker et al. indicate that thrust is only weakly affected. In the case of kinetic afterburning, the results presented from analysis and experiments by Stalker et al. indicate that there is some loss in thrust when burning is incomplete at the exit of the combustor and continues in the nozzle.

For highly engine-integrated scramjet-powered vehicles, the nozzle design can strongly influence the performance of other components of the vehicle. Starkey and Lewis [13] and Starkey [14] investigated optimizing the design of hypersonic scramjet-powered vehicles and considered the design tradeoffs including nozzle design. They included multiple-engine designs and the implications for structural mass and packaging. In this study, the important consequential effects of changes in the nozzle design on the overall vehicle performance are included. To ensure that the force-prediction methodology developed in Tanimizu et al. [6] is applicable for the type of design changes being considered, a scramjet vehicle was manufactured and tested in the T4 shock tunnel. It is of interest to investigate the performance of the designs over a range of flow conditions. Some improvements in the design of the vehicle tested in Tanimizu et al. [6] were also made before the nozzle-optimization study. The next sections detail the design of that scramjet and the results from the tunnel tests. The optimization study and results are then presented in Secs. VI and VII.

II. Test Models

In this paper, quasi-axisymmetric scramjet vehicles are investigated. A primary advantage of this type of vehicle is its large centerbody volume that can be used to carry the payload and fuel. The geometry is also amenable to simplified analysis. The model tested in the present study is 1 in.a series of models tested in the T4 shock tunnel. Figure 1 shows 3-D CAD drawings of three of these models, showing the development of aspects of their design. The vehicle of Paull et al. [3], referred to as model 0, is shown in Fig. 1a and that of Tanimizu et al. [6], referred to as model 1, is shown in Fig. 1b. Both were designed for Mach 6 conditions. Model 1 was derived from model 0 by altering the nozzle and cowl. The test model for the present study, referred to as model 2, is shown in Fig. 1c and was designed for Mach 8 conditions. This was also derived from model 0, but the higher design Mach number of 8 was chosen. The forebody cone angle was 9 deg for all models. Stalker [15] indicates that if a fixed-geometry scramjet operates over a wide range of flight Mach numbers, a scramjet designed for a higher operating Mach number would be expected to give better overall performance than one designed for the lower end of the operating range. Mach 6, 8, and 10 shock-tunnel nozzles were available to test scramjet models in the T4 shock tunnel. So the Mach 8 design condition allows the model to be tested both below and above the design Mach number.

Several modifications to the basic design of models 0 and 1 were incorporated into model 2 to try to improve the performance of the scramjet. These variations are detailed next. Other variations could also have been incorporated in the design studies, such as varying the cowl length and the use of plug nozzles.

First, the bevels on the leading edges of the intake cowl for model 2 face toward the inside of the intake rather than toward the outside, as for models 0 and 1. This modification means that the flow that is compressed by the bevelled leading edges of the cowl passes into the combustion chambers rather than being spilled. This compressed gas is then available for thrust production in the nozzle. This will also

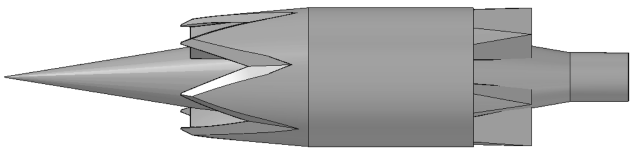

a) Model 0

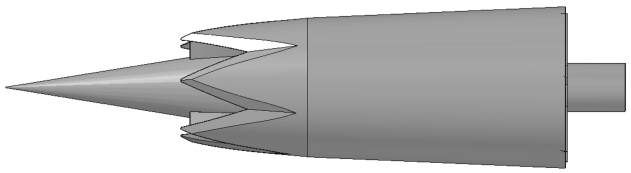

b) Model 1

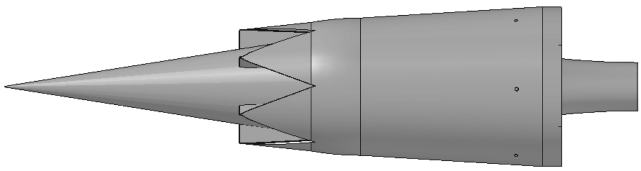

c) Model 2

Fig. 1 Three-dimensional CAD figures of the models 0, 1 and 2.

provide a higher compression ratio for the intake than if the compression was on the outside.

The second major modification from models 0 and 1 is that a shorter and divergent combustion chamber is employed. The results [6] of the force predictions for model 1 indicate that a major source of skin-friction drag is on the walls of the combustion chamber and that the skin-friction drag becomes dominant with increasing Mach number. The combustion chamber of model 2 is designed to reduce skin-friction drag on the combustion chamber surfaces by employing a short combustor. The combustion chamber is only 30 mm long so an ignition promoter, such as silane, would be needed to initiate combustion. Diverging the combustion chamber can prevent thermal and frictional choking [16]. The ratio of the cross-sectional area at the combustor exit to that at the combustor entrance is 1.8. The flow properties inside the combustion chamber for models 1 and 2 for Mach 8 flow conditions for a nozzle-supply enthalpy of 3 MJ/kg are shown in Fig. 2. These are calculated using generalized one-dimensional flow [17]. For the case of no combustion, the Mach number in the combustion chamber of model 1 decreases along the chamber, due to friction, but the Mach number increases in the diverging combustor of model 2. It can be seen that the intake of model 2 produces a higher compression than does that of model 1. The pressure then decreases gradually, due to the divergence in the combustion chamber, but the average pressure level in the combustor of model 2 is still higher than in that of model 1.

The centerbody of model 2 consists of a 9 deg semi-angle conical forebody, and a 11.3 deg semi-angle conical afterbody. The inlets and combustion chamber entrances consist of compression ramps formed by six splitters, which deflect the flow that has already passed through the conical forebody shock wave by a further 8.5 deg. Model 2 has a 3000 mm^2 intake capture area, which is 20% larger than that of model 1. The leading edge of the intake cowl is cut out at an angle of 70 deg. The interior of the intake cowl leading edge has bevels that are at 5 deg to the freestream direction to avoid shock detachment. The slightly divergent combustion chambers are bounded by the side walls, conical afterbody, and cowl. Downstream of the end of the combustion chamber, the splitters deflect the flow through an angle of 7.6 deg and the cowl internal surface deflects the flow through an angle of 6 deg. The 11.3 deg semi-angle conical afterbody forms the inner surface of the thrust nozzles. The nozzle of model 2 is 75 mm long and the external cowl deflection angle is 3.5 deg. The ratio of nozzle exit area to nozzle entrance area is 15.6. The distance from the cone tip to the entrance of the combustion chambers is approximately 180 mm and the complete length of the model is approximately 320 mm.

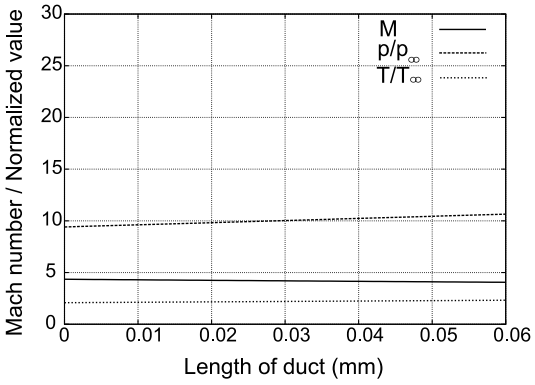

a) One-dimensional flow analysis for model 1

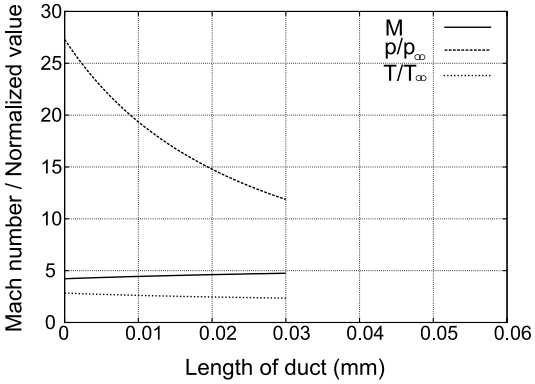

b) One-dimensional flow analysis for model 2

Fig. 2 Flow properties in the different shapes of combustion chambers ($M_\infty = 7.9, p_\infty = 2.6$ kPa, $T_\infty = 230$ K, and $C_f = 0.002$).

III. Force-Prediction Methodology

The force-prediction methodology that was used in the present optimization study is similar to that detailed in [6]. Hence, only a brief description and the differences from the previous modeling are given here. Drag force is produced by the tangential (viscous) and normal (pressure) forces acting on the surfaces of the test model exposed to flow. The total drag force has been calculated by addition of the contributions from each component. The methods used to calculate the inviscid forces on the conical forebody, intake and cowl are similar to those used by Paull et al. [3]. The viscous drag due to laminar boundary layers is calculated using a reference temperature method. The effective boundary-layer running length is used to determine the boundary-layer state (laminar or turbulent). The transition Reynolds number was determined from a correlation obtained in a study of transition in the T4 shock tunnel by He and Morgan [18]. The viscous drag for turbulent boundary layers is calculated by the theory of van Driest [19] when the Reynolds number exceeds the transitional Reynolds number. The boundary layers in the combustion chambers and nozzles were assumed to be turbulent, because it is expected that the disturbances caused by the crossing shocks generated by the splitters of the intakes will induce transition [20]. The conditions in the combustion chamber and the nozzle were determined using the in-house CFD code, EILMER [21] run in inviscid mode with viscous forces calculated separately [6].

Since the intake of model 2 is different from that of models 0 and 1, the theoretical modeling of the intake flow was changed appropriately. The modeling of the flow in the intake is shown schematically in Fig. 3. First, the conditions on the inside surface of the cowl are calculated by finding the conditions downstream of the shock wave from the bevel and then passing this flow through the shock wave generated by the splitter. Second, the flow conditions on the splitter surface are divided into two regions (see Fig. 3a). The flow conditions in region 1 are taken as those for flow that has passed

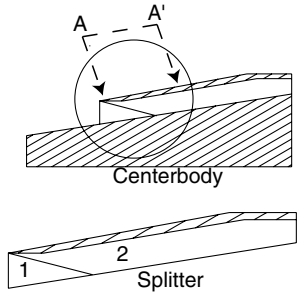

a) Surface on the splitter

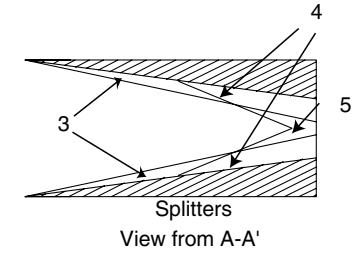

b) Surface on the centerbody

Fig. 3 Shock-wave structures in the intake for model 2.

through the oblique shock wave generated by the splitter. The flow conditions in region 2 are calculated by passing the flow first through the shock wave from the splitter and then accounting for the additional compression generated by the bevels. Finally, the flow conditions on the centerbody surface are divided into three regions (see Fig. 3b).The flow conditions in region 3 are calculated by passing the oncoming flow through the oblique shock from the splitter.

The flow conditions in region 4 are obtained by taking the flow in region 3 and accounting for the additional compression from the bevel. The flow conditions in region 5 are computed by taking the condition across the oblique shock from the bevel. The flow entering the combustion chamber is not uniform, due to shocks and expansion waves. The problem can become complex and a simple solution is sought. Paull et al. [3] applied an adiabatic stream tube analysis to calculate equivalent uniform conditions that could be used at the entrance to the combustion chamber. They calculate the conditions that would exist for an adiabatic 1-D flow from the intake capture area to the total cross-sectional area of the combustion chamber. The analysis includes an allowance for entropy changes across the crossing shock waves [22].

IV. Validation of Theoretical Modeling

Experiments performed in the T4 stalker tube [4] at the University of Queensland were used to validate the modified theoretical modeling. Three different (Mach 6, 8, and 10) tunnel nozzles [23–25] were used to produce a range of test flows for the current study. All measurements in this paper were conducted after the test flow was fully established. Flow establishment time includes nozzle starting time and the boundary-layer establishment time. The former was up to 1 ms for the lower enthalpy conditions and shorter for the higher-enthalpy conditions and the latter was taken as the time required for the flow to traverse 3.3 body lengths [26]. The determination of the test time obtained for each shot in the T4 shock tunnel is the same as that detailed in Tanimizu et al. [6]. All measurements reported here were taken after flow establishment and before the end of the steady test flow. The initial test gas temperature and pressure in the shock tube, the measured nozzle-supply pressure, and the measured speed of the primary shock wave down the shock tube were used to determine the test flow conditions using codes STN [27], ESTC [28], and NENZF [29]. The details of the performance of the three tunnel nozzles used in this study are shown in [23–25,30]. A single component stress wave force balance [31] was used to measure the drag forces acting on the model. This force measurement technique is able to measure the pressure forces and viscous forces acting on a test model during the very short duration of a shock-tunnel test [31–33]. Drag coefficients were then computed with the measured drag forces. The vertical lines in Figs. 4–6 indicate that the 95% confidence interval uncertainty in the measured drag coefficient determined from following the procedure in [34]. The drag coefficients measured for model 2 in the Mach 8 nozzle tests are plotted as a function of the nozzle-supply enthalpy in Fig. 4. As the nozzle-supply enthalpy increases, the unit Reynolds number of the flow decreases and the Mach number of the flow from the shock-tunnel nozzle decreases. These effects are shown on the horizontal axis of the plot. Both experiment and theory show the same trend of increasing drag coefficient with increasing nozzle-supply enthalpy although the variations in the experimental values are close to being within the uncertainty limits. The theoretical and experimental results generally agree to within experimental uncertainty, but there is a tendency for the measured drag coefficient to increase somewhat more rapidly with nozzle-supply enthalpy than is indicated by the theoretical calculations.

To investigate the performance at offdesign conditions, the drag coefficients measured for model 2 for the Mach 6 and 10 nozzle tests are plotted as a function of nozzle-supply enthalpy in Figs. 5 and 6. For model 2 the forebody shock wave was not captured completely by the cowl for all conditions in the Mach 6 nozzle tests. A background-oriented schlieren (BOS) image [35] of the flow around model 2 is shown in Fig. 7. For this condition the freestream Mach number was 6.2 and nozzle-supply enthalpy was 5.8 MJ/kg. This is below the design Mach number of 8 for model 2. It is seen that the forebody shock wave generated at the tip of cone is not captured at this condition. An oblique shock wave generated at the crotch of the cowl can be seen also. Therefore, some of the compressed flow was spilled over the cowl. This spillage then affects the overall performance of model 2. The effect of the spillage is included in the theoretical methodology by modeling the flow over the cowl as that behind the forebody shock. Drag coefficients approximately 5%

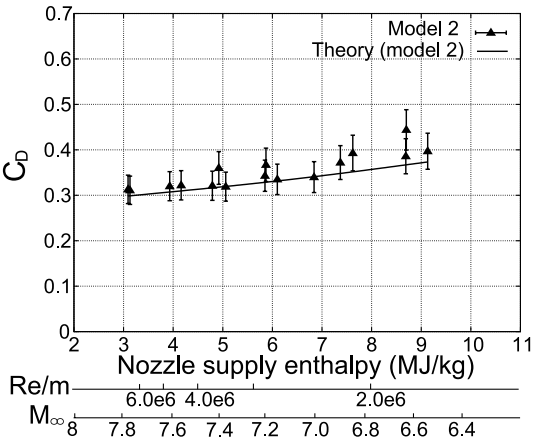

Fig. 4 Drag coefficients for tests with the Mach 8 nozzle for model 2.

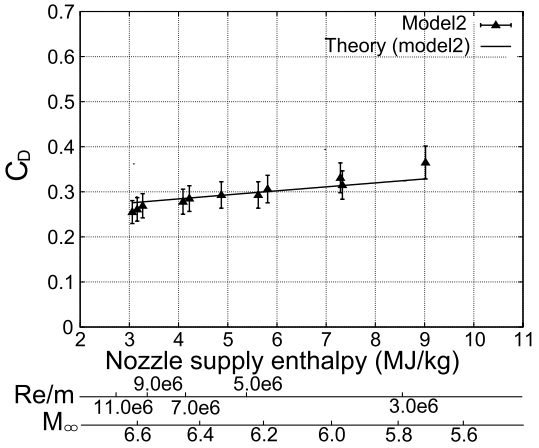

Fig. 5 Drag coefficients for tests with the Mach 6 nozzle for model 2.

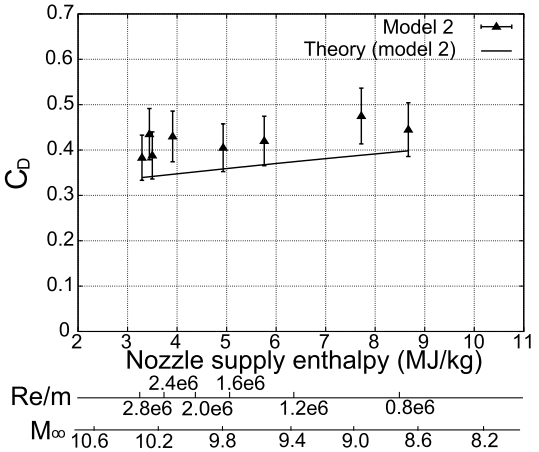

Fig. 6 Drag coefficients for tests with the Mach 10 nozzle for model 2.

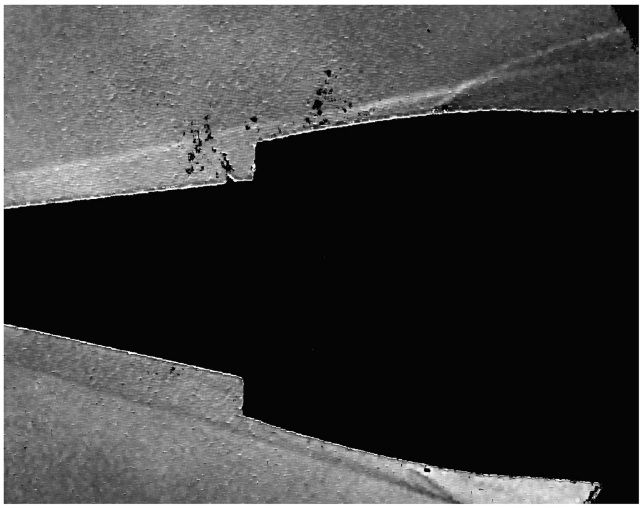

Fig. 7 BOS picture of model 2, shot No 9417, 5.8 MJ/kg, $M_\infty = 6.2$.

lower than those in Fig. 5 are obtained if this effect is neglected. For the Mach 6 test cases, the theoretical predictions are slightly higher than those measured at lower nozzle-supply enthalpies, but the theoretical predictions agree with measurements to within experimental uncertainty over the range of nozzle-supply enthalpies tested.

For the tests in the Mach 10 nozzle, the theory consistently underpredicts the drag coefficient, as was the case for model 1 (see [6]). This may be due to a stronger influence of swept oblique shock-wave boundary-layer interactions [36] caused by the splitters at the relatively low Reynolds numbers for the Mach 10 nozzle tests. The boundary layers are expected to be laminar on the centerbody at the splitters for all tests with the Mach 10 nozzle and skewed shocks are more likely to induce laminar boundary-layer separation [20] than for turbulent boundary layers. However, the theoretical and experimental results show similar trends. Some measurements differ from the theoretical prediction by more than the uncertainties in the measurements.

The major factor influencing the drag coefficient is the Reynolds number. This can be seen by plotting the measured drag coefficients as a function of the freestream unit Reynolds number, see Fig. 8. A reduction of the drag coefficients is observed with increasing Reynolds number. In the theoretical calculations, the boundary layers in the combustor and nozzle are treated as turbulent and the turbulent skin-friction drag coefficient decreases monotonically with increasing Reynolds numbers. At similar Reynolds numbers (e.g., around 4×10^6) the tests with different tunnel nozzles produce similar drag coefficients. A closer investigation of the results from modeling shows that as the Mach number increases, the contribution to pressure drag coefficient is similar, due to the competing effects of decreasing intake drag and decreasing nozzle thrust. The result is that variation of the drag coefficient for this model depends mainly on the contributions of skin-friction drag.

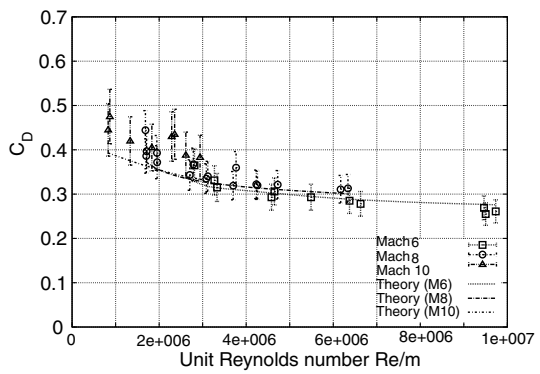

Fig. 8 Overall performance for model 2 (Reynolds number effect).

V. Nozzle-Optimization Study

The Nelder and Mead simplex method [37] was used in the optimizer. A coarse mesh ($40 \times 20 \times 20$ cells) was used for the inviscid nozzle-flow calculations to reduce the calculation time required for each iteration in the optimization. This mesh size was determined to be suitable from a mesh refinement study. After the optimization routine had located the optimum solution a finer mesh ($80 \times 40 \times 40$ cells) was used to calculate the final forces for the optimized shape.

As discussed in the Introduction, the objective function in the present study was the net drag coefficient of the complete vehicle. It is appropriate for an airbreathing engine to use the intake capture area as the reference area in the drag coefficient. The net drag coefficient for the nozzle and cowl was calculated using

$$C_D = [F_p + F_v + \mathrm{CFD}_{\mathrm{results}}]/(0.5 \times \rho U^2 A_i) \tag{2}$$

where F_p is the pressure drag on the cowl external surface, F_v is the skin-friction drag on the cowl's external surface and $\mathrm{CFD}_{\mathrm{results}}$ is the axial force on the nozzle calculated using EILMER. F_p and F_v were obtained using the force-prediction methodology [6]. Note that there will be additional mass required for longer nozzles and that this has not been accounted for in the current optimization study.

VI. Results of Optimization and Parametric Studies

A. Parametric Study for Mach 8 Flow Conditions

The first step in the optimization study was to vary the key parameters in the nozzle design to investigate their influence on performance and to verify that the optimization code can successfully identify the lowest drag design. The optimization code used in this study is a local search method that can potentially capture only a local minima. A parametric study is a good way to check that the global minimum is found and it also shows how much the performances of the designs vary as the parameters are changed. A previous scramjet nozzle-optimization study conducted by Jacobs and Craddock [10] indicates that the effect of the centerbody shape is limited. Their optimized nozzle produces only 8% more thrust than a simple straight ramp nozzle for the same area ratio nozzle. Therefore, the major nozzle design parameters that influence the overall performance of a quasi-axisymmetric scramjet of the form studied here are expected to be the length of the nozzle and the external deflection angle of the cowl (see Fig. 9).

An axial cross-section of the combustion chamber and nozzle taken midway between the splitters is shown in Fig. 9a. The geometry of the nozzle is specified by six points. Points C, D, E, and F are fixed. Point A can move in both the axial X and radial R directions. Point B is fixed at the same radius as the sting and is at the same X location as point A.

The length of the nozzle, measured from the end of combustor (see Fig. 9), was varied from 35 to 155 mm in steps of 10 mm. The

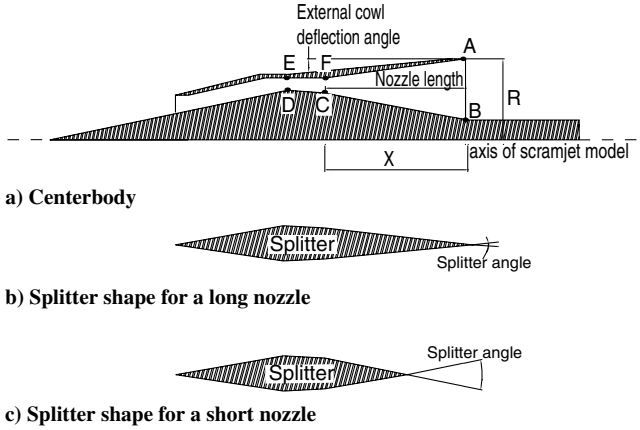

Fig. 9 Parameters for nozzle study.

Table 1 Flow conditions for optimization and parametric studies

Conditions	Values
Freestream	
Velocity, m/s	2392.0
Mach	7.9
Static pressure, kPa	2.65
Static temperature, K	230.0
Static density, kg/m^3	0.040
Combustion chamber (entrance)	
Velocity, m/s	2200.0
Static pressure, kPa	71.0
Static temperature, K	653.0
External flow	
Mach	7.52
Static pressure, kPa	3.0
Static temperature, K	250.0
Static density, kg/m^3	0.041

external deflection angle of the cowl was varied from 0 deg to 10 deg in 1 deg increments. These ranges were chosen by considering the size limitations of the test core flow in T4. Correspondingly, the shape of the splitter was changed as the nozzle length changed. This is shown in schematically in Figs. 9b and 9c. Note that a shorter nozzle will have a large splitter deflection angle (see Fig. 9c).

For the parametric study, the freestream was set at a Mach number of 7.9, static temperature of 230 K and static pressure of 2.65 kPa. Since the size of the test models are limited by the size of the test core flow, the tunnel conditions are at higher-pressure conditions than the flight conditions using $\rho\ L$ scaling [38]. Thus, the model test conditions are equivalent to the flight conditions at an altitude of approximately 30 km [39] for a vehicle 2.2 times the size of a model that could be tested in the T4 Stalker tube. It is noted that the equivalent flight conditions are likely to require a combustion igniter such as silane for these conditions. The flow conditions at entry to the combustion chamber and the conditions for the flow over the external surface on the cowl were obtained using the force-prediction methodology [6] with the modifications described in this paper. Table 1 shows these conditions.

As the nozzle length and external cowl deflection angle are varied, the area ratio of the nozzle, defined as A_{exit}/A_c, varies. A_c is the cross-sectional area at entry to the combustion chamber and A_{exit} is the cross-sectional area at exit of the nozzle. The way that A_{exit} varies for the chosen ranges of these parameters is shown in Fig. 10. As can be seen, the area ratio varies from approximately 12 to 46.

Contours of the overall vehicle drag coefficient are shown in Fig. 11. The white square shows the estimated location of the optimum design. The estimated minimum drag coefficient is 0.28 at Mach 8 flight condition. The white zone shows the region of over-expanded conditions where the flow is expected to separate in the nozzle, due to overexpansion.

The conditions for which flow separation takes place within thrust nozzles and the locations of separation are reported in the literature (see, e.g., [40]). The nozzle-flow separation criterion of Summerfield

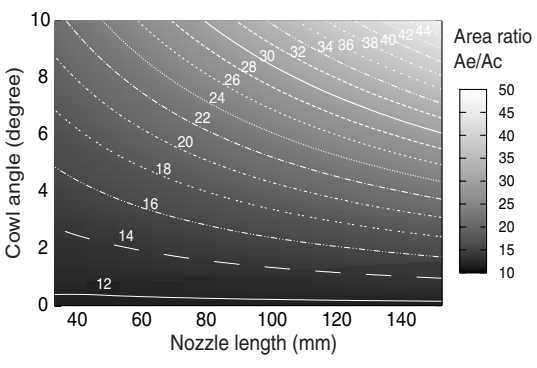

Fig. 10 Area ratio (A_{exit}/A_c) from parametric study.

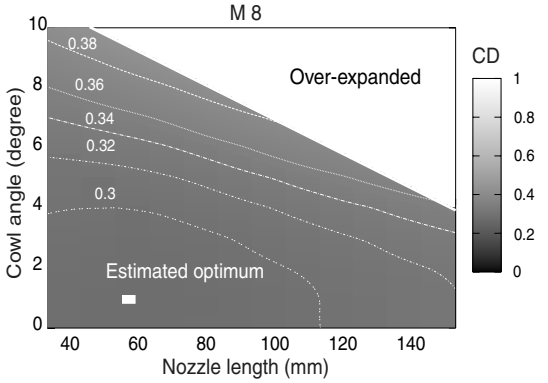

Fig. 11 Results from parametric study for Mach 8 condition (fuel off).

et al. [41] was used in this study. This simplest approach has limitations, as discussed by other researchers (e.g., Kalt and Badal [42], Morrisette and Goldberg [43] and Romine [44]), but is considered to be adequate for the present purpose. Therefore, there might be some small errors involved in the estimated drag coefficient. For an axisymmetric nozzle, they found that flow separation occurred for pressure ratios p_s/p_a between 0.34 to 0.40, where p_a is the static pressure into which the nozzle-flow exhaust and p_s is the static pressure at which separation occurs. For the present study, incipient separation was assumed to occur when $p_s/p_a \equiv 0.37$. This pressure level (p_s/p_a) was calculated using generalized one-dimensional flow analysis including area change and effects of friction [17]. Using this criterion, the maximum nozzle area ratio for which a nozzle would expand the flow without separation is 23.1 for the present flow conditions at entry to the nozzle.

As can be seen in Fig. 11, the objective function is well behaved and has only one minimum. The force-prediction methodology provides a breakdown of the viscous and inviscid forces acting on different parts of the vehicle. An examination of the components of the drag coefficient from the force-prediction methodology shows that the thrust from the nozzle increases with increasing cowl angle and length. The drag coefficient also increases with increasing external cowl deflection angle and length. For nozzle lengths from 35 to 65 mm and external cowl deflection angles from 0 to 1 deg, the increase in nozzle thrust outweighs the increase in drag, due to the cowl deflection. This causes the overall drag coefficient of the vehicle to decrease. However, for higher cowl deflection angles, the drag coefficient increases with increasing angle. The drag also increases with increasing nozzle length.

The results indicate that the benefit from incorporating a larger area ratio and longer nozzle is limited for this type of scramjet engine. The optimum nozzle is about 60 mm long with an external cowl deflection angle of approximately 1 deg. The area ratio of this nozzle is approximately 13.

B. Optimization for Mach 8 Conditions

This section describes the results of the study to optimize the nozzle shape for the Mach 8 condition. The optimization method of Nelder and Mead [37], that is used here, is suitable for optimizing functions of many variables. However, more function evaluations are required for more variables and there are some cases where the optimum may not be found. The optimization procedure for the

Table 2 Breakdown C_D for models A1 and 2

	Model A1	Model 2
	Area ratio 12.4	Area ratio 15.6
Thrust	−0.078	−0.092
Pressure drag on intake and cowl	0.255	0.277
Skin-friction drag on intake and cowl	0.051	0.054
Skin-friction drag on combustion chamber and nozzle	0.053	0.058
Total drag coefficient	0.281	0.297

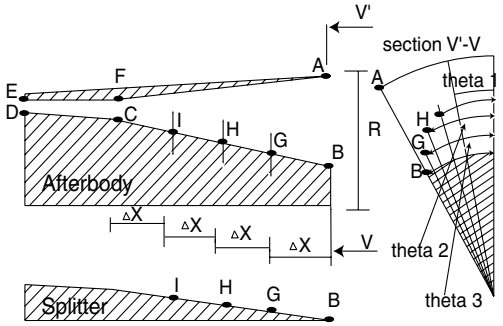

Fig. 12 Configuration of final optimization study.

current application was conducted using the following steps. Firstly, an initial optimization was conducted. Two main parameters were varied in the first step—the nozzle length and the external cowl deflection angle. Then the shapes of the model centerbody and the splitters to produce maximum thrust for the nozzle length and external cowl angle determined from the first step in the optimization study were found in a second optimization step.

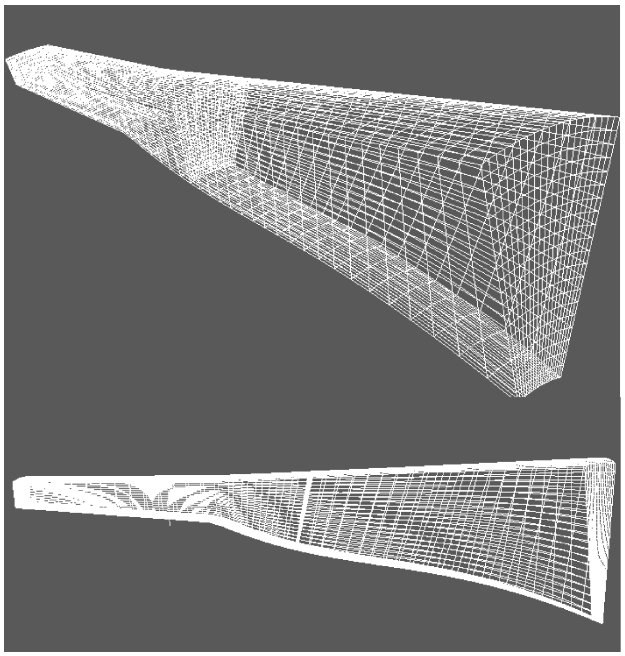

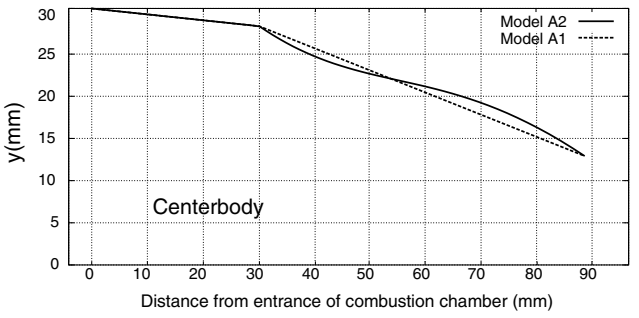

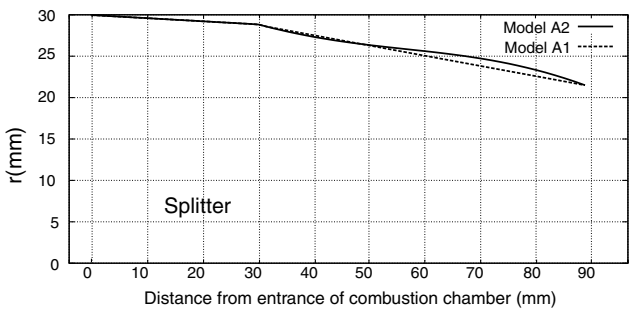

Fig. 13 Optimized shapes of nozzle centerbody and splitters.

1. Optimization Step 1: Nozzle Length and External Cowl Deflection Angle

The starting geometry of the nozzle was that of model 2. (See Fig. 1c.) After 450 iterations, the optimizer converged to a solution. This optimized scramjet vehicle is referred to as model A1. The optimum nozzle length and external cowl deflection angle were found to be 58.0 mm and 0.75 deg, respectively. The area ratio of the nozzle is 12.4. This is close to the optimum point identified in the parametric study, giving confidence that the optimization code was able to find the correct optimum.

It is of interest to identify the drag and thrust forces from different components for the optimized shape. Table 2 shows a breakdown of the components of drag coefficient for models A1 and 2 for $M_\infty = 7.9$, $p_\infty = 2.65$ kPa, $T_\infty = 230$ K and $\rho_\infty = 0.04$ kg/m^3. The thrust coefficient of model A1 is smaller than that of model 2 because of the smaller area ratio of the nozzle of model A1, but the overall drag coefficient of model A1 is smaller than that of model 2. The main contribution to the reduced drag is the reduced external pressure drag on the cowl.

2. Optimization Step 2: Nozzle Shape

The nozzle length and external cowl deflection angle determined from the first step of the study were fixed in this step of the optimization study. The nozzle internal shape was changed using three Bezier points [45] in an attempt to improve the performance of the nozzle. Usually, nozzles with curved surfaces, such as bell-shaped nozzles, achieve higher performance than nozzles with simple straight surfaces, such as conical nozzles [46].

The Bezier points used to define the shape of the centerbody, H, G, and I (see Fig. 12) were located at equal distances, Δx, apart. The Bezier points were free to move in both the R and θ directions (see Fig. 12).

After 400 iterations, the optimizer converged to a solution. The optimized scramjet is referred to as model A2. The optimized nozzle for the Mach 8 flow condition is shown in Fig. 13. The general shape of the optimized centerbody is similar to that from the optimization study performed by Jacobs and Craddock [10]. They used a full Navier–Stokes solver, whereas the current study used the combination of an inviscid CFD model and simple viscous theory.

Table 3 Breakdown C_D for models A1 and A2

	Model A1	Model A2
	Area ratio 12.4	Area ratio 12.4
Thrust	−0.078	−0.080
Pressure drag on intake and cowl	0.255	0.255
Skin-friction drag on intake and cowl	0.051	0.051
Skin-friction drag (C.C and nozzle)	0.053	0.055
Total drag coefficient	0.281	0.280

Table 4 Flow conditions for parameter studies (offdesign)

	Mach 6	Mach 7	Mach 9	Mach 10
Freestream				
Velocity, m/s	1778	2080	2686	2990
Mach	5.9	6.9	8.9	9.9
Combustion chamber				
Velocity, m/s	1546	1877	2484	2794
Static pressure, kPa	68.4	68.7	99.3	103.5
Static temperature, K	604.8	622.0	738.6	778.7
Outside flow				
Mach	5.7	6.60	8.60	9.5
Static pressure, kPa	3.1	3.1	2.6	2.6
Static temperature, K	243.6	246.1	244.0	248.5
Static density, kg/m^3	0.040	0.040	0.040	0.040

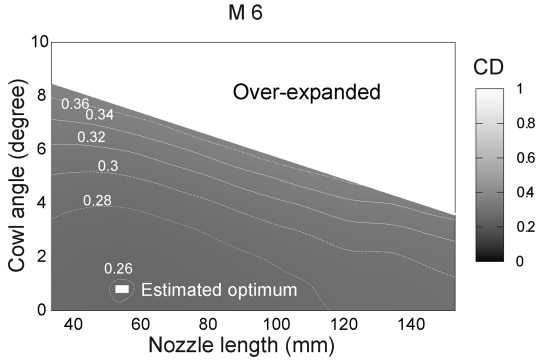

a) Mach 6 condition

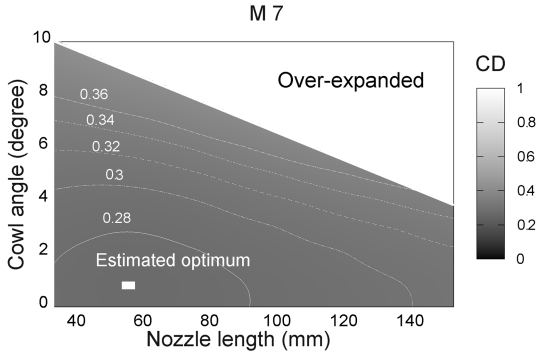

b) Mach 7 condition

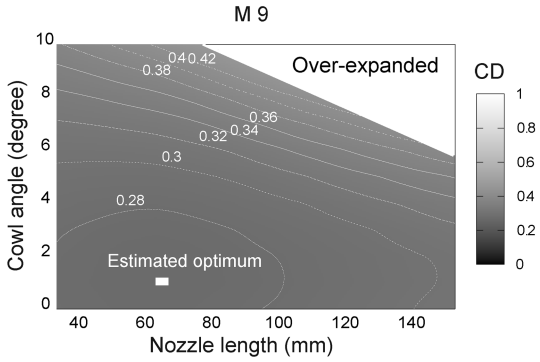

c) Mach 9 condition

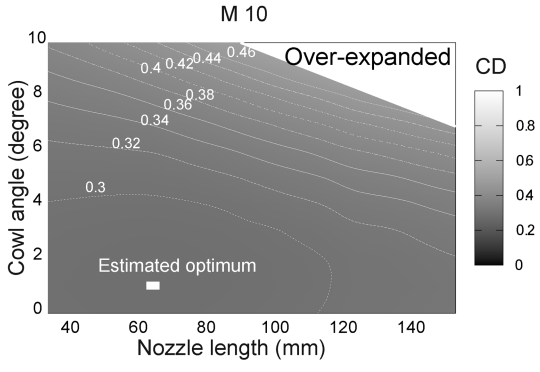

d) Mach 10 condition

Fig. 14 Results from parametric studies for offdesign conditions.

This gives further confidence in the suitability of the current method for nozzle optimization.

The shapes of the centerbodies and splitters in the nozzles for models A1 and A2 are compared at the bottom of Fig. 13. The general shapes are similar to those found by Jacobs and Craddock [10] for 2-D optimized scramjet thrust nozzle designs. The optimized geometry gave only a 0.5% reduction of the overall drag coefficient from that of model A1. Table 3 shows the breakdown of the components of the drag coefficient for models A1 and A2 at the design condition. The thrust coefficient from the nozzle of model A2 is only a modest 3% larger than that for model A1. It is noted that a longer nozzle has more potential for thrust increase by changing centerbody shape because of the greater opportunity for wave cancellation. However, skin-friction drag will also be higher in longer nozzles. The skin-friction drag coefficient in the combustion chamber and the nozzle for model A2 is 2% larger than that for model A1.

Table 5 Results from parametric studies (offdesign)

	Mach 6	Mach 7	Mach 9	Mach 10
Nozzle length, mm	55.0	55.0	65.0	65.0
Cowl deflection angle deg	1.0	1.0	1.0	1.0
Thrust	−0.139	−0.101	−0.091	−0.075
Pressure drag on intake and cowl	0.282	0.265	0.248	0.25
Skin-friction drag on intake and cowl	0.052	0.051	0.048	0.051
Skin-friction drag (C.C and nozzle)	0.064	0.056	0.065	0.060
Total drag coefficient	0.260	0.271	0.270	0.285

C. Parametric Studies for Various Mach Numbers

The effects of changes in the flight Mach number on the performance of the model were investigated. The optimization study for Mach 8 conditions presented in the previous sections shows that the main parameters affecting the performance of the quasi-axisymmetric scramjet are the nozzle length and the external cowl deflection angle. Therefore, these parameters were varied and the overall performances were calculated for Mach numbers of 6, 7, 9, and 10. The nozzle length was varied from 35 to 155 mm in steps of 10 mm and the external cowl deflection angle was varied from 0 to 10 deg in steps of 1 deg.

Table 4 shows the flow conditions for these parametric studies. Note that Mach number and velocity are changed for offdesign freestream conditions. Pressure, temperature and density are the same as those for the Mach 8 condition. This was done to investigate the effect of varying flight speed at a fixed altitude. The results of the parametric studies for these offdesign conditions are shown in Figs. 14a–14d. The white square shows the location of the estimated optimum for each condition. The white zones show the regions where the nozzles are overexpanded to such an extent that separation is expected according to Summerfield et al.'s [41] nozzle-flow separation criteria.

The estimated optimum length of the nozzle increases from approximately 55 mm for the Mach 6 condition to approximately 65 mm for Mach 10 condition, giving the expected result that a longer nozzle is more advantageous when a scramjet operates at higher flight Mach numbers. The optimum angle of the cowl varies little from around 1 deg as the flight Mach number varies from 6 to 10.

The main results from this part of the study are summarized in Table 5. The contribution of skin-friction drag coefficient to the overall drag does not vary much over the range of Mach numbers considered, but the performance of the nozzle dramatically decreases with increasing Mach number. Therefore, the net drag coefficients increase with increasing Mach numbers.

VII. Conclusions

Parametric and optimization studies for the design of a Mach 8 scramjet nozzle were performed using computational fluid dynamics and simple theories adapted from Tanimizu et al. [6]. The Nelder and Mead algorithm [37] was used in the optimization studies. The optimization study for the scramjet-powered vehicle was conducted at Mach 8 flight conditions for an altitude of 30 km. The results of the optimization study for fuel-off conditions indicate that a short nozzle with a small external cowl deflection angle (55 mm long and around

1 deg) is good for fuel-off conditions, but improvement of the performance of the model was not significant.

The main goal of this paper was to investigate the improvement of the overall performance by improving the nozzle performance. The key factors for improving the nozzle performance are the nozzle area ratio and length. However, the optimization results indicate that the overall performance of the vehicle cannot be increased just by increasing the nozzle area ratio because of the implications for external drag on the cowl. The basic geometry of this quasi-axisymmetric scramjet design means that a large external cowl deflection angle is required to attain a large nozzle area ratio. This large external cowl deflection angle produces additional pressure drag. Therefore, the benefit of improving nozzle performance by extending the cowl is balanced by the production of additional external drag on the cowl. This implies that other techniques will be required to improve the performance of a scramjet of this design. For example, it may possible to reduce the drag internally by techniques such as boundary-layer combustion [47] in order to achieve better overall performance without compromising the nozzle performance.

Acknowledgments

This work was supported by the Australian Research Council through Discovery Project DP0452374. The authors would like to thank James Turner, Andrew Ridings, Sarah Razzaqi, Thomas Jazra, and Rainer Kirchhartz for their assistance during the experiments. Thanks also to Keith Hitchcock for modifications to the test models and to Dwishen Ramanah for setting up the visualization system.

References

[1] Hartfield, R. J., Burkhalter, J. E., and Jenkins, R. M., "Scramjet Missile Design Using Genetic Algorithm," *Applied Mathematics and Computation*, Vol. 174, No. 2, 2006, pp. 1539–1563. doi:10.1016/j.amc.2005.07.003

[2] Earl, A. H., and Ernest, M. A., "NASA's Hypersonic Research Engine Project—A Review," NASA TM-107759, 1994.

[3] Paull, A., Mee, D. J., and Stalker, R. J., "Experiments on Supersonic Combustion Ramjet Propulsion in a Shock Tunnel," *Journal of Fluid Mechanics*, Vol. 296, 1995, pp. 159–183. doi:10.1017/S0022112095002096

[4] Stalker, R. J., "Free-Piston Shock Tube," *Aeronautical Quarterly*, Vol. 17, No. 4, Nov. 1966, pp. 351–370.

[5] Smart, M. K., and White, J. A., "Computational Investigation of the Performance and Back-Pressure Limits of a Hypersonic Inlet," AIAA Paper 2002-0508, Jan. 2002.

[6] Tanimizu, K., Mee, D. J., Stalker, R. J., and Jacobs, P. A., "Drag Force on Quasi-Axisymmetric Scramjets at Various Flight Mach Numbers: Theory and Experiment," *Shock Waves*, Vol. 19, No. 2, 2009, pp. 83–93. doi:10.1007/s00193-009-0194-x

[7] Colville, J. R., Starkey, R. P., and Lewis, M. J., "Axisymmetric Inlet Design for Combined-Cycle Engines," *Journal of Propulsion and Power*, Vol. 22, No. 5, 2006, pp. 1049–1058. doi:10.2514/1.18063

[8] Matthews, A. J., Jones, T. V., and Cain, T. M., "Design and Test of Hypersonic Isentropic-Spike Intake with Aligend Cowl," *Journal of Propulsion and Power*, Vol. 21, No. 5, 2005, pp. 838–843. doi:10.2514/1.13000

[9] Valorani, M., Nasuti, F., Onofri, M., and Buongiorno, C., "Optimal Supersonic Intake Design for Air Collection Engines (ACE)," *Acta Astronautica*, Vol. 45, No. 12, 1999, pp. 729–745. doi:10.1016/S0094-5765(99)00185-X

[10] Jacobs, P. A., and Craddock, C. S., "Simulation and Optimization of Heated, Inviscid Flows in Scramjet Ducts," *Journal of Propulsion and Power*, Vol. 15, No. 1, 1999, pp. 73–81. doi:10.2514/2.5393

[11] Stalker, R. J., Paull, A., Mee, D. J., Morgan, R. G., and Jacobs, P. A., "Scramjets and Shock Tunnels The Queensland Experience," *Progress in Aerospace Sciences*, Vol. 41, No. 6, 2005, pp. 471–513. doi:10.1016/j.paerosci.2005.08.002

[12] Stalker, R. J., Truong, N. K., Morgan, R. G., and Paull, A., "Effects of Hydrogen-Air Non-Equilibrium Chemistry on the Performance of a Model Scramjet Thrust Nozzle," *The Aeronautical Journal*, Vol. 108, No. 1089, 2004, pp. 575–584.

[13] Starkey, R. P., and Lewis, M. J., "Critical Design Issues for Airbreathing Hypersonic Waverider Missiles," *Journal of Spacecraft and Rockets*, Vol. 38, No. 4, 2001, pp. 510–519. doi:10.2514/2.3734

[14] Starkey, R. P., "Scramjet Optimization for Maximum Offdesign Performance," AIAA Paper 2004-3343, 2004.

[15] Stalker, R. J., "Waves and Thermodynamics in high Mach Number Propulsive Ducts," *High-Speed Flight Propulsion System*, edited by E. T. Curran, and S. N. B. Murthy, Vol. 137, Progress in Astronautics and Aeronautics, AIAA, Reston, VA, 1991, pp. 237–264.

[16] Tomioka, S., Kobayashi, K., Kudo, K., Murakami, A., and Kanda, T., "Performance of Supersonic Combustors with Fuel Injection in Diverging Section," *Journal of Propulsion and Power*, Vol. 22, No. 1, 2006, pp. 111–119. doi:10.2514/1.16041

[17] Shapiro, A. H., *The Dynamics and Thermodynamics of Compressible Fluid Flow*, 1st ed., Wiley, New York, 1953.

[18] He, Y., and Morgan, R. G., "Transition of Compressible High Enthalpy Boundary Layer Flow over a Flat Plate," *The Aeronautical Journal*, Vol. 98, No. 25, 1994, pp. 25–34.

[19] van Driest, E. R., "Problem of Aerodynamic Heating," *Aeronautical Engineering Review*, Vol. 15, No. 10, 1956, pp. 26–41.

[20] Degrez, G., and Ginoux, J. J., "Surface Phenomena in a Three-Dimensional Skewed Shock Wave/Laminar Boundary-Layer Interaction," *AIAA Journal*, Vol. 22, No. 12, 1984, pp. 1764–1769. doi:10.2514/3.8849

[21] Jacobs, P. A., and Gollan, R. J., "The Eilmer3 Code: User Guide and Example Book," Univ. of Queensland, School of Mechanical and Mining Engineering, Rept. 2008/07, Brisbane, Australia, 2009.

[22] Hall, N. A., *Thermodynamics of Fluid Flow*, Prentice–Hall, Upper Saddle River, NJ, 1951.

[23] Overton, S., and Mee, D. J., "T4's M5 and M8 Nozzle Pitot Rake Survey," *4th International Workshop on Shock Tube Technology*, Brisbane, Australia, 20–24 Sept. 1994.

[24] Knell, M., "Calibration of a Mach 7.6 Nozzle," Univ. of Queensland, Div. of Mechanical Engineering, Rept. 2003/13, Brisbane, Australia, 2003.

[25] Abdel-Jawad, M. M., "The Mach 10, 30 Km Altitude Condition in the T4 Shock Tunnel Using a New Mach 10 Nozzle," Univ. of Queensland, Div. of Mechanical Engineering, Rept. 2005/5, Brisbane, Australia, 2005.

[26] Jacobs, P. A., Rogers, R. C., Weidner, E. H., and Bittner, R. D., "Flow Establishment in a Generic Scramjet Combustor," *Journal of Propulsion and Power*, Vol. 8, No. 4, 1992, pp. 890–899. doi:10.2514/3.23566

[27] Krek, R. M., and Jacobs, P. A., "STN, Shock Tube and Nozzle Calculations for Equilibrium Air," Univ. of Queensland, Div. of Mechanical Engineering, Rept. 2/93, Brisbane, Australia, 1993.

[28] McIntosh, M. K., "Computer Program for the Numerical Calculations of Frozen and Equilibrium Conditions in Shock Tunnels," Australia National Univ., Rept. CR-181721, Canberra, Australia, 1968.

[29] Lordi, J. A., Mates, R. E., and Moselle, J. R., "Computer Program for the Numerical Solution of Nonequilibrium Expansions of Reacting Gas Mixtures," NASA CR-472, 1966.

[30] Jacobs, P. A., and Stalker, R. J., "Mach 4 and Mach 8 Axisymmetric Nozzles for a High-Enthalpy Shock Tunnel," *The Aeronautical Journal*, Vol. 95, No. 949, 1991, pp. 324–334.

[31] Sanderson, S. R., and Simmons, J. M., "Drag Balance for Hypervelocity Impulse Facilities," *AIAA Journal*, Vol. 29, No. 12, Dec. 1991, pp. 2185–2191. doi:10.2514/3.10858

[32] Tuttle, S. L., Mee, D. J., and Simons, J. M., "Drag Measurements at Mach 5 Using a Stress Wave Force Balance," *Experiments in Fluids*, Vol. 19, No. 5, 1995, pp. 336–341. doi:10.1007/BF00203418

[33] Rowan, S. A., and Paull, A., "Performance of a Scramjet Combustor with Combined Normal and Tangential Fuel Injection," *Journal of Propulsion and Power*, Vol. 22, No. 6, Nov.–Dec. 2006, pp. 1334–1338. doi:10.2514/1.18744

[34] Mee, D. J., "Uncertainty Analysis of Conditions in the Test Section of the T4 Shock Tunnel," Univ. of Queensland, Div. of Mechanical Engineering, Rept. 1993/4, Brisbane, Australia, 1993.

[35] Ramanah, D., Raghunath, S., Mee, D. J., Rösgen, T., and Jacobs, A. P., "Background Oriented Schlieren for Flow Visualisation in Hypersonic Impulse Facilities," *Shock Waves*, Vol. 17, No. 1–2, Aug. 2007, pp. 65–70. doi:10.1007/s00193-007-0097-7

[36] Mee, D. J., Stalker, R. J., and Stollery, J. L., "Glancing Interactions Between Single and Intersecting Oblique Shock Waves and a Turbulent Boundary Layer," *Journal of Fluid Mechanics*, Vol. 170, Sept. 1986,

pp. 411–433.
doi:10.1017/S0022112086000952
[37] Nelder, J. A., and Mead, R., "A Simplex Method for Function Minimization," *Computer Journal*, Vol. 7, No. 4, 1965, pp. 308–313.
doi:10.1093/comjnl/7.4.308
[38] Hornung, H. G., "28th Lanchester Memorial Lecture–Experimental Real-Gas Hypersonics," *The Aeronautical Journal*, Vol. 92, No. 920, 1988, pp. 75–85.
[39] White, F. M., "Physical Properties of Fluids," *Fluid Mechanics*, 6th ed., McGraw–Hill, New York, 2008, App. A, p. 818.
[40] Arens, M., and Spiegler, E., "Shock-Induced Boundary Layer Separation in Overexpanded Conical Exhaust Nozzles," *AIAA Journal*, Vol. 1, No. 3, 1963, pp. 578–581.
doi:10.2514/3.1598
[41] Summerfield, M., Foster, C. R., and Swan, W. C., "Flow Separation in Overexpanded Supersonic Exhaust Nozzles," *Jet Propulsion*, Vol. 24, No. 5, 1954, pp. 319–321.
[42] Kalt, S., and Badal, D., "Conical Rocket Nozzle Performance Under Flow-Separated Conditions," *Journal of Spacecraft and Rockets*, Vol. 2, No. 3, 1965, pp. 447–449.
doi:10.2514/3.28200
[43] Morrisette, E. L., and Goldberg, T. J., "Turbulent-Flow Separation Criteria for Overexpanded Supersonic Nozzles," NASA TP-1207, 1978.
[44] Romine, G. L., "Nozzle Flow Separation," *AIAA Journal*, Vol. 36, No. 9, 1998, pp. 1618–1625.
doi:10.2514/2.588
[45] Prautzsch, H., Boehm, W., and Paluszny, M., *Bézier and B-Spline Techniques*, 1st ed., Springer, Berlin, 2002.
[46] Sutton, G. P., "Nozzle Theory and Thermodynamic Relations," *Rocket Propulsion Elements: An Introduction to the Engineering of Rockets*, 6th ed., Wiley, New York, 1992, pp. 41–88.
[47] Stalker, R. J., "Control of Hypersonic Turbulent Skin Friction by Boundary-Layer Combustion of Hydrogen," *Journal of Spacecraft and Rockets*, Vol. 42, No. 4, 2005, pp. 577–587.
doi:10.2514/1.8699

J. Powers
Associate Editor